Volume Transport Variability on the Northern Argentine Continental Shelf from In Situ and Satellite Altimetry Data

L. S. Lago[1,2,3], M. Saraceno[1,2,3], A. R. Piola[2,4], L. A. Ruiz-Etcheverry[1,2]

[1] Centro de Investigaciones del Mar y la Atmósfera (CIMA-CONICET/UBA), Buenos Aires, Argentina. [2] Departamento de Ciencias de la Atmósfera y de los Océanos, FCEN, Universidad de Buenos Aires, Buenos Aires, Argentina. [3] Unidad Mixta Internacional-Instituto Franco-Argentino para el Estudio del Clima y sus Impactos (UMI-IFAECI/CNRS-CONICET-UBA), Buenos Aires, Argentina. [4] Departamento de Oceanografía, Servicio de Hidrografía Naval (SHN), Buenos Aires, Argentina.

Corresponding author: Loreley S. Lago (cima.fcen.uba.ar)

Key Points:

- The time averaged along-shore transport in the northern Argentine is 2.65 Sv to the northeast, with a peak-to-peak range of 16 Sv.
- Satellite altimetry data can be used to infer the along-shore transport variability at time scales longer than 20 days.
- The variability of the Malvinas Current modulates the along-shore transport only in the outer 30 km of continental shelf.

This article has been accepted for publication and undergone full peer review but has not been through the copyediting, typesetting, pagination and proofreading process, which may lead to differences between this version and the Version of Record. Please cite this article as doi: 10.1029/2020JC016813.

Abstract

Direct current observations and satellite altimetry data over the northern portion of the Argentine continental shelf are used to produce an 11-month long hourly time series and a 25-year long daily time series of along-shore volume transport, respectively. At time scales longer than 20 days, the temporal variability of the in situ transport is significantly correlated with the transport inferred from satellite altimetry (r = 0.74). The mean in situ along-shore transport is 2.65 ± 0.07 Sv (1 Sv = 10^6 m^3 s^{-1}) to the northeast and presents large variability, with a peak-to-peak range of 16 Sv. The extended satellite transport presents variability at multiple time scales. The annual cycle is the dominant signal, with a maximum during the austral autumn and a minimum during the austral spring. The interannual component of the transport is significantly correlated (r = -0.5) with the Southern Annular Mode (SAM). SAM-induced along-shore wind stress anomalies over the region modulate the cross-shore pressure gradient that, in turn, modulates the along-shore transport variability. This mechanism holds also at synoptic scales, highlighting the dominant role of the wind on the along-shore transport. Satellite altimetry measurements also indicate that the cross-shore pressure gradient generated by the variability of the Malvinas Current affects the along-shore transport only in the outer 30 km of the continental shelf.

Plain Language Summary

The Argentine continental shelf is a vast region of more than one million m^2, whose circulation has been mostly studied through hydrographic data and numerical simulations. Here, we present the first estimate of the along-shore transport over the northern Argentine continental shelf based on direct velocity measurements. Transport is also computed using bottom pressure and coastal tide gauge observations, and satellite altimetry data. We produced an 11-month long hourly time series and a 25-year long daily time series of along-shore transport. Results show that the satellite transport represents accurately the in situ transport at time scales longer than 20 days. The in situ transport has a mean value of 2.65 ± 0.07 10^6 m^3 s^{-1} to the northeast and large variability, with a range of 16 Sv. Satellite transport is dominated by the annual cycle, with a maximum during the austral autumn and a minimum during the austral spring. Its interannual component is related to the Southern Annular Mode (SAM), responsible for along-shore wind anomalies that modulate the transport variability. Satellite altimetry data also indicates that the

Malvinas Current affects the along-shore transport only in the outer 30 km of the continental shelf.

1 Introduction

Though continental shelves host large primary productivity and contribute significantly to the carbon balance of the global ocean, in many regions the dynamics of the shelf circulation and its temporal variability are still poorly understood. The Argentine Continental Shelf (ACS) hosts one of the most productive ecosystems of the world ocean and abundant fishing resources of commercial relevance (Auad & Martos, 1998; Acha et al., 2004; Romero et al., 2006; Álvarez-Colombo et al., 2011), whose life cycles are modulated by physical processes. The environmental variability modulates the primary production which, in turn, is transferred to higher trophic levels (Bakun, 1996). Therefore, improved understanding of the regional circulation variability and its drivers are essential to better understand the dynamics of the shelf circulation and its possible impact on the species distribution. Given the dynamical constraints imposed by the bottom topography, the cross-shelf transports are small compared to the along-shelf transports (e.g. Brink, 2016). Thus, the along-shelf volume transport is the most basic metric of the shelf circulation. This manuscript presents the first estimate of the along-shore transport over the ACS based on direct current measurements, bottom pressure and coastal tide gauge observations, and satellite altimetry data.

The ACS is located in the Southwest Atlantic Ocean between 55°S and 35°S, between the coast and the 200 m isobath. Computing transport over this broad region is a complex task, the shelf circulation is subject to a large tidal amplitude in the southernmost region, strong variable winds (Palma *et al*., 2008), and a complex bathymetry. The scarce number of direct velocity observations available over this wide continental shelf prevents the accurate determination of the along-shore volume transport. Therefore, so far, the circulation has been largely inferred from hydrographic data (Guerrero and Piola 1997; Piola and Rivas, 1997), mass and heat conservation arguments (e.g. Rivas, 1994), and from numerical model simulations (Palma et al., 2008; Combes & Matano, 2018). These studies showed that the circulation over the ACS is characterized by a North-Northeastward flow of subantarctic water modified by continental discharge and low-salinity water from the Pacific Ocean that arrives to the ACS through the Magellan Strait (Piola et al., 2000; Brun et al., 2020). Recent analyses of direct current

observations near 39°S showed that, once the tidal signal is removed, the along-shore wind stress largely accounts for the variability of the along-shore circulation for periods ranging between 7 and 15 days (Lago et al., 2019). Lago et al. (2019) also showed that the along-shore circulation is largely barotropic and uniform in the cross-shore direction. Models suggested that the circulation over the shelf is influenced by local wind stress and also by the barotropic pressure gradients generated by the intense, northward flowing Malvinas Current along its offshore boundary (Palma et al., 2008; Matano et al., 2010).

In this work, we compute the along-shore volume transport using in situ data, and extend the transport time series with satellite altimetry data. Satellite altimetry products provide useful information to explore the time variability of the ocean circulation over wide regions but are generally more reliable in the open ocean. However, during the past decade substantial progress has been made correcting Sea Surface Height (SSH) errors in coastal and shelf regions (Vignudelli et al., 2011). In particular, over the ACS, several studies have relied on satellite altimetry to characterize the seasonal and interannual time scales and spatial patterns of the geostrophic circulation (Saraceno et al., 2014; Strub et al., 2015; Ruiz-Etcheverry et al, 2016; Lago et al., 2017). For example, Strub et al. (2015) and Ruiz-Etcheverry et al. (2016) showed that altimetry can resolve the circulation at seasonal time scales. These studies found that geostrophic currents inferred from satellite altimetry data flow equatorward with a slight seasonality, with stronger variations in the inner shelf, and mean values increasing towards the shelf break. Saraceno et al. (2014) showed that altimetry data display the expected seasonality of the extension of the Rio de la Plata plume along the Uruguay and southern Brazil coasts, while Lago et al. (2017) showed that along-track satellite altimetry is accurate within 12 cm up to 2 km from the coast as long as an adequate procedure to reprocess the radar signal is applied. Lago et al., (2017) used ALES retracking (Passaro et al., 2014) and the tidal model that best represented tides in their coastal region of study, within the ACS.

The main objective of this study is to compute and analyze the temporal variability of the along-shore volume transport over the ACS based on an 11-month record of direct current observations and near-bottom pressure measurements, and also 25 years of daily satellite altimetry data. The in situ data were collected within the French-Argentine CASSIS project (http://www.cima.fcen.uba.ar/malvinascurrent/en/) which consisted on two mooring arrays deployed along two sections of the ACS, spanning from the coast up to the 200 m isobath. To the

best of our knowledge, the velocity measurements obtained within the CASSIS project are the longest records obtained so far in the ACS and therefore, offer a unique opportunity to improve our understanding of the regional circulation. The location of the CASSIS moorings used in this study are displayed in Figure 1. Given the barotropic nature and the cross-shelf coherency of the along-shore flow reported by Lago el al. (2019), the available data may be used to provide a robust estimate of the volume transport over the continental shelf.. The following sections of the paper present the data sets considered and the methods used for the analysis (Section 2), the results and discussions (Section 3) and main conclusions (Section 4).

2 Data and Methods

2.1 In situ data

In situ data used in this work were collected by three moorings deployed within the CASSIS project. Moorings A1 and A2 consist of recoverable frames that were deployed at the bottom during 11 months (December 2014 – November 2015) over a cross-shelf section of the ACS near 39ºS under track #26 of Jason 2 satellite altimeter (Figures 1 and 2). Mooring A1 was located 60 km from the coast, at 70 m depth, and mooring A2, 154 km from the coast, at 90 m depth. Each mooring was equipped with an upward-looking 300 KHz Acoustic Doppler Current Profiler (ADCP) along with temperature (T), salinity (S) and pressure (P) sensors. All instruments were configured to record hourly data (Table 1). ADCPs provided zonal and meridional currents at 4 m vertical bins, the first beam was 6 m above the sea bottom and we used data up to 10 m from the sea surface for A1 and up to 12 m for A2 to avoid surface contamination of the velocity measurements, mostly due to air bubbles. T, S and P sensors were installed 0.6 m above the sea bottom. Further description and an analysis of these data can be found in Lago et al. (2019) and are publicly available (Saraceno et al., 2019). The third mooring was an oceanographic buoy that operated during 42 days near the shelf break and that measured velocities with a downward-looking 190 kHz ADCP recording hourly velocity data over 10 m bins (Table 1). Buoy measurements are reported in Paniagua et al. (2018) and are available in Saraceno et al. (2017). We also use hourly sea level measurements from 17 December 2014 to 21 November 2015 from the coastal tidal gauge (TG) located at Mar del Plata (Table 1, Figures 1 and 2) that is part of the NOAA network Global Sea Level Observing System (GLOSS). TG data

were kindly provided by the Servicio de Hidrografía Naval (SHN). To remove the tidal signal present in all the in situ measurements (Lago et al., 2019), we applied a low-pass filter with a cut-off period of 48 h.

2.2 Satellite altimetry data

Altimetry data are essential for long-term analyses of the oceanic conditions as they provide reliable SSH measurements since 1993. The reprocessing of the radar signal and the application of different corrections allowed the use of satellite SSH over coastal regions (e.g. Birol et al., 2017; Vignudelli et al., 2011; Cipollini et al., 2017). Coastal altimetry data has been thoroughly validated in the ACS and have proved to represent accurately seasonal and longer period oscillations (Lago et al., 2017; Ruiz-Etcheverry et al., 2016; Ruiz-Etcheverry et al., 2015; Strub et al., 2015; Saraceno et al., 2008). Nonetheless, no comparison was carried out so far between geostrophic velocities derived from satellite altimetry and direct velocity observations in the ACS. Here, we evaluate two altimetry-derived velocity products by comparing them with the in situ velocity measurements. The good agreement between these data (Section 3.2) allows us to estimate the transport using velocities inferred from satellite altimetry and hence obtain a 25-year time series of the along-shore transport (see methodology in Section 2.4).

The two satellite altimetry datasets considered are a gridded multi-satellite product and the along-track data collected over track #26 of the Jason 2 satellite mission. The along-track data is a 1 Hz product, which results in one SSH observation every 6 - 7 km along the track. The ALES along-track data has a temporal resolution of 10 days and is distributed by the Deutsches Geodätisches Forschungsinstitut Technische Universität München Center (TUM, https://openadb.dgfi.tum.de/en/). The gridded satellite product merges several satellite missions that are interpolated to a homogeneous grid. These data are produced by the Archiving, Validation and Interpretation of Satellite Oceanographic (AVISO) and distributed by the Copernicus Marine and Environment Monitoring Service (CMEMS, https://www.marine.copernicus.eu). The gridded product has a 1/4º x 1/4º spatial resolution and a daily temporal resolution. It is important to note that the gridded product merges different satellite missions whose temporal resolution is 10 days or more. The effective spatial and temporal resolution of the gridded product has been estimated as 280 km and 28 days (Ballarotta

et al., 2019). In Section 3.3 we show that the highest correlation between the in situ velocities and the satellite-derived geostrophic velocities for the gridded product is attained when the former is low-pass filtered with a cut-off period of 20 days, in good agreement with results obtained further offshore, within the MC (Ferrari et al., 2017).We worked with the gridded data between 1 January 1993 through 31 December 2017. The comparison of the two satellite-derived surface velocities described above with the in situ data described in Section 2.1 is presented in Section 3.3.

2.3 Reanalysis data

We use sea level pressure (SLP) data for the computation of geostrophic velocities from in situ P measurements and wind stress data to analyze the variability of the estimated transport time series. SLP and wind stress were obtained from the ERA-Interim reanalysis, which consists of a 40 years global analysis of atmospheric fields and is based on an assimilation system included in a numerical model. ERA-Interim is produced by the European Center of Middle-range Weather Forecast (ECMWF, https://www.ecmwf.int/). We consider daily SLP and wind stress data with a 3/4º x 3/4º spatial resolution (Berrisford et al., 2009). The choice of this data set is based on a comparison of different wind products with in situ wind measurements obtained at the oceanographic buoy deployed at the shelf break (Lago et al., 2019, Figure 1).

2.4 Methodology

To compute the along-shore transport, we select the along-shore velocities that pass across the vertical section that extends from the coast to the 200 m isobath following track #26 of J2 satellite mission (Figure 2). Three methods are applied to estimate the transport: two methods are based on in situ data and the third one, on satellite data.

Hereinafter, the transport estimate based on ADCP velocities is referred to as direct transport; the transport estimate based on geostrophic velocities inferred from the TG SSH and bottom pressure time series at A1 and A2 is referred to as indirect transport; and the transport estimate based on geostrophic velocities derived from satellite altimetry data is referred to as

satellite transport. In the following, we first describe the velocity time series and then we explain the methods applied to compute the volume transport.

2.4.1 In situ direct velocities

We use the barotropic component of the direct velocity measurements in all locations. The barotropic component is estimated as the vertical average of the velocity measurements. We do not consider the upper 30 m of the water column in this calculation to exclude the ageostrophic velocities within the surface Ekman layer. The along-shore Ekman transport along the analyzed section has a mean value of 0.04 ± 0.12 Sv and represents 0.3% of the total transport estimated from the direct method, computed in Section 2.4.4.

The barotropic component of the direct velocities explains 84% of the total variance at A1 and A2 (Lago et al., 2019) and 66% of the total variance at the oceanographic buoy. Although the buoy produced only a 42 day time series, we extend it to the 11-month record length obtained at A1 and A2 thanks to the fact that the along-shore barotropic components of the buoy and of A2 are significantly correlated (0.6 at a 95% confidence level, Figure S1). To this end, we first compute the best linear fit between the along-shore velocity at the buoy and at A2 and then extend the buoy time series to the 11-month period based on the A2 record. The data available at the buoy correspond to summer 2015, when the water column is stratified. To determine if the relationship between the along-shore velocity at A1 and A2 varied as a function of the seasonal changes in the vertical stratification, we computed the correlations in summer and winter and found a non-significant difference (0.87 in summer and 0.9 in winter). Though this result suggests that the seasonal stratification that characterizes the continental shelf from A1 to the buoy (Lago et al., 2019) does not affect the correlation between the barotropic component at A1 and A2, additional observations in the outer shelf are necessary to improve the reliability of the along-shore transport over the shelf.

2.4.2 In situ geostrophic velocity

We compute the along shore geostrophic velocity component from in situ data following equation 1:

$$u = -\frac{g}{f}\frac{\partial SSH}{\partial y} \qquad (1)$$

Where *u* represents the along-shore geostrophic velocity, *f* is the Coriolis parameter, *g* the acceleration of gravity, *y* denotes the cross-shore direction and SSH is the sea surface height. SSH is available at the TG and is computed from the bottom pressure measurements at A1 and A2. To obtain the SSH at A1 and A2 we assume the hydrostatic balance, correct the bottom P with the sea-level pressure from ERA-Interim reanalysis, and use a seasonal estimate of the density, as in Lago et al. (2019). We then obtain two mid-point estimates of geostrophic velocity using the three SSH time series and equation (1): one from the SSH gradient between TG and A1 (Vg_a) and the other from the SSH gradient between A1 and A2 (Vg_b). Each of these time series represents the averaged flow between each pair of SSH observations (Figure 2b). As Vg_a and Vg_b are relative geostrophic velocities, it is necessary to add a reference velocity to obtain an absolute geostrophic velocity: we add the time averaged barotropic velocity of A1 to Vg_a and the average barotropic velocity of A1 and A2 to Vg_b. Adding a reference velocity to the relative geostrophic velocity inferred from SSH gradients introduces 2 problems (Meinen et al., 2010): i) the presence of an ageostrophic component in the velocities used as a reference; ii) the fact that the relative geostrophic velocities represent an average between the two sites where pressure was observed, while the direct velocity observations are representative of a single point. Fortunately, in this region these two problems are minor because: i) the main ageostrophic component is within the Ekman layer, which is not included in the estimate of the reference velocity; and ii) Vg_a and Vg_b are highly correlated to the barotropic velocities at A1 and A2, respectively (Lago et al., 2019). Therefore, the direct velocities are representative of a wider extension and not only of the point of measurement. As will be shown later, the excellent agreement between the direct and indirect velocity variability, which are fully independent, suggests that our indirect method works remarkably well.

2.4.3 Satellite geostrophic velocities

The selected along-track data provides SSH measurements every 7 km that are usually smoothed along the track to improve the signal to noise ratio (Strub et al., 1997). We tested cut-off wavelengths from 30 km to 100 km before computing the geostrophic velocities following equation 1. The best agreement with the barotropic in situ velocities was obtained with a 30 km

low-pass filter. For the gridded product, we first interpolated the gridded SSH to the along-track section and then computed the along-shore absolute geostrophic velocity from equation 1.

2.4.4 Direct transport

The barotropic component of the along-shore velocity from the ADCPs and the extended velocity time series of the oceanographic buoy described above are used to estimate the direct transport. Given that there is a cross-shore homogeneity in the along-shore velocities, the estimated transport is not sensitive to the choice of the areas over which each velocity is integrated. The three areas considered are shown in Figure 2a. The direct transport over the whole section results from the addition of the transport estimates along the three areas considered.

2.4.5 Indirect transport

The indirect transport estimate is based on the dynamic method explained in Meinen & Watts (2000), in which geostrophic velocities are determined from hydrographic data as explained earlier. The geostrophic velocities considered are Vg_a, for Area1_2, and Vg_b, for Area2_2 (Figure 2b). The total indirect shelf transport results from the addition of the transport calculated over these two sub-areas. A weakness in this approach is the extrapolation of Vg_b to the shelf-break due to the lack of a bottom pressure recorder at the location of the buoy. To compute the error associated with this method we use the bottom pressure recorders intrinsic error (0.4 cm) and the one associated to the TG at Mar del Plata (1 cm). Propagating those instrumental errors, we obtain a transport error for this method of 0.07 Sv.

2.4.6 Satellite transport

As will be shown later in Section 3.2, the satellite geostrophic velocity derived from the gridded SSH product compares better with the in situ velocities than the velocity inferred from the along-track SSH product. Hence, we use the gridded satellite velocities to compute the

satellite transport. Since altimetry data are available since 1993, the satellite transport time series is computed from January 1993 to December 2017.

3 Results and discussion

3.1 In situ volume transport: large variability induced by local wind stress

The time series of the in situ transport computed with the direct and indirect methods are displayed in Figure 3. Both transport time series present similar variability and reach the highest correlation at lag 0 (0.95, 95% CL). It is important to note that, apart from the mean values, these time series are fully independent. Their agreement is strong evidence of the robustness of the assumptions implied in the formulation of the indirect method. Moreover, the similarity between the two in situ transport estimates clearly shows that the variability of the along-shore transport can be determined from a few bottom pressure recorders and the Mar del Plata TG, without the need of a denser sampling array of moorings.

The mean value of the in situ transport is 2.65 Sv for the direct method and 2.21 Sv for the indirect method. Although the absolute geostrophic velocities are determined to match the observed vertically averaged velocities and the total areas considered for both methods are the same, the indirect and direct transports differ because the sub-areas used are different and also because of the extrapolation of Vg_b to the shelf-break in the indirect method. These time averages of the along-shore transports are nearly twice as large as the 1.3 Sv estimated by Forbes and Garraffo (1988) based on the density and wind fields and the 0.9 Sv estimated by Palma et al. (2008) through a section close to 40ºS based on a numerical simulation; and is in somewhat better agreement with the more recent 1.7 Sv estimated by Combes & Matano (2018), also based on a numerical model.

Mean values are small compared to the large variability observed in Figure 3: the peak-to-peak range oscillates between -5 Sv (southwestward, 25 August 2015) and 11 Sv (northeastward, 22 June 2015). Figure 3 also shows that the along-shore volume transport is positive (northeastward) most of the time and that negative values (southwestward flow reversals) are less frequent (7% of the 11-month long record). The reversal events are evenly distributed throughout the year, have a short duration (typically less than 2 days) and can reach

up to -5 Sv. Only on two occasions the flow reversals lasted more than 2 days: in late April 2015 (4 days duration) and in May 2015 (6 days duration). Such reversals may play a significant role in the distribution of planktonic species (Auad and Martos, 2012).

A spectral analysis of the in situ transport time series (Figure S2) shows energetic fluctuations centered between 2 and 5 days, which suggest a link with synoptic-scale wind fluctuations. Indeed, the variability of the along-shore currents is strongly modulated by the cross-shore pressure gradient generated by the along-shore component of the wind stress (Lago et al., 2019). The strong shelf transport response to along-shore winds is readily apparent over the inner and mid-shelf (Figure 4). The correlation coefficient between wind stress and transport fluctuations is larger in the inner shelf (0.7, Figure 4 a) than further offshore (0.6, Figure 4 b and c). This suggests that the cross-shore pressure gradient caused by the along-shore wind stress decays as the distance from the coast increases, as might be expected from Ekman dynamics (e.g. Simpson & Sharples, 2012). Conversely, other processes, as the influence of the MC variability, may have a stronger impact on the strength of the along-shore circulation in the outer shelf. This possibility will be discussed in Section 3.5.

3.2 To what extent satellite derived velocities may be used to estimate volume transport over the ACS?

In this section we evaluate to what extent satellite altimetry derived velocities may be used to estimate the volume transport in the region and hence extend the transport time series to the full period of available satellite altimetry data (i.e. from 1993). The results described in the previous section suggest that the vertically averaged along-shore currents in the ACS are in approximate geostrophic balance. Furthermore, Lago et al. (2019) showed that the velocity variance is only weakly dependent of depth and that the barotropic component represents nearly 90% of the total variance. Therefore, we compare satellite-derived velocities with the barotropic component of the along-shore in situ velocities (Figure S3). Two satellite products are evaluated: the along-track Jason 2 and the multi-satellite gridded data described in Section 2. The comparison is carried out only for the dates when J2 along-track data is available, that is every 10 days. Results show that the correlation coefficients are higher for the gridded product than for the along-track data (Figure S3), and that only the correlation coefficients of the gridded product

with in situ data are significant (95% CL). This result suggests that the velocity derived from the gridded product provides a more realistic representation of the circulation. The in situ velocity measurements show similar variability and the dominant oscillations coincide with meteorologically forced motions (7 to 15 days). This indicates that the higher temporal resolution of the gridded altimetry product, that results from the combination of different satellite missions, provides more useful information to accurately represent the observed circulation than the higher spatial resolution of the along-track product.

The best comparison between directly observed and satellite derived geostrophic velocities is found when a low-pass filter of 20 days is applied to the data. A similar conclusion was obtained at the shelf break over the same satellite altimetry track (Ferrari et al., 2017). Table 2 presents the correlation coefficient and the RMSD between in situ and gridded velocities for the complete period with a time span of 1 day. Results show that the lowest RMSD values and highest correlation coefficients are found as the distance from the coast increases. From these results, we conclude that there is a reasonably good agreement between the along-shore components of the in situ and satellite velocities inferred from the gridded SSH product, particularly in the mid-shelf region. In what follows, we estimate the along-shore transport using the geostrophic velocities provided by the gridded satellite product as explained in section 2.2.

3.3 Satellite transport: mean and seasonal variability

The satellite velocity is inferred from the SSH, computed as the Sea Level Anomaly (SLA) plus the Mean Dynamic Topography (MDT). Therefore, inaccuracies in the MDT can lead to inaccuracies in the velocity, and consequently, can lead to inaccuracies in the satellite-derived transport. The gridded maps of SSH produced by AVISO that we considered so far use the MDT computed by Rio et al. (2011). To test if better results can be obtained with a different MDT, we recomputed the satellite-derived geostrophic velocity using three different MDTs: Maximenko MDT (Maximenko et al., 2009), the DTU MDT (Andersen et al., 2015) and CNES2018 MDT, produced by Collecte Localization Satellite (CLS) and available at https://www.aviso.altimetry.fr. The comparison of the absolute geostrophic velocities inferred from satellite SSH with the in situ measurements show that, at A1, the best match is obtained with the DTU MDT, while at A2, the best match is obtained with Maximenko's MDT (Table

S1). We then computed the along-shore satellite-derived transport using the four selected MDTs: the mean satellite transport along the section is closer to the mean in situ direct transport when using CNES2018 MDT (Figure S4 and Table S2). It is important to note that the mean value using CNES2018 MDT is similar to the mean value using Rio et al. (2011), they differ in only 0.14 Sv. In the following, the analysis of the along-shore component of the satellite transport is carried out using CNES2018 MDT for the period from 1993 to 2017 (Figure 5b). In 2015 this satellite-derived transport is in good agreement with the 20-day lowpass filtered in situ transport (Figure 5a): the correlation coefficient between both transports is 0.74 (95% CL) and the RMSD is 0.6 Sv. The mean and standard deviation of the satellite transport are 2.42 Sv and 0.64 Sv, while the mean and standard deviation of the direct transport are higher: 2.65 Sv and 0.77 Sv. The difference between in situ and satellite mean transports (0.23 Sv) cannot be attributed only to the instrumental error (0.07 Sv, see Section 2). We argue that the difference is related to inaccuracies in the MDT. The extended transport time series ranges between 0.4 and 5.5 Sv, with a record-length mean value and standard deviation similar to those obtained during 2015 with satellite data: 2.42 Sv and 0.64 Sv. The 20-day filtering required to best match the in situ and satellite derived transports implies a substantial reduction of the peak-to-peak transport variability (e.g. Figures 3 and 5). Consequently, no transport reversals are apparent in the filtered in situ and satellite data in 2015 (Figure 5a), nor in the entire satellite record (Figure 5b). However, low transport events in the filtered data, such as the ~1 Sv in mid-May 2015 (Figure 5a) are clearly associated with transport reversals as suggested by the -4 Sv in the non-filtered in-situ transport (Figure 3). Thus, minima in the satellite derived transport (Figure 5b) are likely associated with transport reversals of relatively short duration, as the ones observed during 2015. This is in agreement with recent reports of a transport reversal event in October 2013 detected by hydrographic and lowered ADCP observations obtained near 37°S (Berden et al., 2020). This event was produced by persistent northeasterly winds and is also readily apparent as a minimum (0.5 Sv) in our satellite time series (Figure 5b). As pointed out in Auad & Martos (2012), Lago et al. (2019), and Berden et al. (2020), these reversal events might have strong biological consequences, since they can influence the distribution of planktonic species.

A spectral analysis of the extended satellite transport time series shows that the variability is dominated by the annual cycle and, to a lower extent, by oscillations of periodicities

that spread between 12 days and 2 months (Figure 6). We associate the intra-seasonal oscillations to atmospheric variability (see Section 3.1). To further explore the annual cycle, we compute the monthly-mean climatology of the satellite transport (Figure 7a). The climatology presents a maximum in austral autumn (~3.0 Sv in April) and a minimum in austral spring (~1.8 Sv in October) that differs from the along-shore wind stress climatology (Figure 7b). Combes & Matano (2018) observed maxima and minima for the same months, however their maximum monthly transport is 2.2 Sv. Not surprisingly, the transport climatology obtained is also in good agreement with the annual cycle of the satellite SLA distributions (Ruiz-Etcheverry et al., 2016). The climatological SLA maps show a cross-shore gradient that corresponds to a positive along-shore transport throughout the year whose amplitude is in phase with our transport estimate (Ruiz-Etcheverry et al., 2016). This agreement might be expected, since both seasonal cycle estimates are based on satellite altimetry data. Ruiz-Etcheverry et al. (2016) also showed that the cross-shore SLA gradient is due to the fact that, close to the coast, the steric height is maximum in April and minimum in October, corresponding respectively to a stronger and weaker northeastward transport.

Finally, it is worth noting that the monthly-mean satellite transport estimate during 2015 differs from the long-term climatology computed from satellite data (Figure 7a). The monthly satellite transport exceeds the climatological value plus one standard deviation in September 2015 and is lower than the climatological value minus one standard deviation in July 2015 (Figure 7a). These transport anomalies are consistent with anomalously intense along-shore wind stress over the region (Figure 7b). Thus, we argue that the interannual variability of the seasonal component of the along-shore transport is modulated by changes in the intensity of the along-shore wind stress. In the following section we further explore the interannual component of the satellite transport time series.

3.4 Satellite transport: interannual variability

To further investigate the nature of the interannual variability of the satellite transport we first subtract the seasonal cycle from the total transport time series. The seasonal cycle is computed trough harmonic analysis of the transport time series. Then, we applied a low-pass filter with a cut-off period of 18 months to the residual time series and compared it with two

climate indexes: the Southern Annular Mode (SAM) index and the Southern Oscillation Index (SOI) as provided by the National Oceanic and Atmospheric Administration (NOAA, https://www.esrl.noaa.gov). The SAM index is representative of the circumpolar average of zonal atmospheric pressure difference between 65°S and 40°S (Marshall, 2003) and is the leading mode of variability in the southern hemisphere atmospheric circulation on monthly and interannual timescales. The interannual along-shore transport is inversely correlated (-0.5, 95% CL) with the SAM index (Figure 8) and directly correlated to the interannual along-shore component of the wind stress (0.5, 95% CL; Figure S5). Between 37°S and 40°S, when the SAM is in its positive phase, it induces a weakening of the southwesterly winds; while when the SAM is in its negative phase, it induces a strengthening of the southwesterly winds. These wind anomalies produce a cross-shore pressure gradient due to changes in the SSH that modulates the intensity of the along-shore transport. A similar argument to explain the interannual variability of the transport was provided over the southern portion of the Patagonia continental shelf (Combes and Matano, 2018; Guihou et al., 2020). We also evaluated the transport response to the SOI. The SOI index is related to El Niño and is estimated as the pressure difference between Tahiti and Darwin, Australia. The interannual along-shore transport does not show a significant correlation with the SOI index (not shown). Several studies showed that the influence of the SOI in the Southwestern Atlantic is mostly noticeable in the region affected by the Rio de la Plata river (Piola et al., 2005; Piola et al., 2008; Saraceno et al., 2014).

To characterize the interannual component of the circulation, we compute the Empirical Orthogonal Function (EOF; Preisendorfer, 1998) modes of the interannual SLA over the ACS between 37.5ºS and 40ºS, from the coast up to the 200 m isobath. The interannual component of the SLA was computed following the same methodology explained above for the interannual transport estimate. The first EOF mode explains 62.6% of the SLA variance (Figure S6) and presents very low SLA gradients. Therefore, its influence on the circulation is negligible. An analysis of the possible forcing of this leading mode is presented at the end of this subsection. Here, we analyze the signal of the interannual SLA not associated with the first mode. This residual is computed by subtracting the reconstruction of the leading mode to the interannual time series. A new EOF analysis of the interannual SLA residual (Figure 9) shows that the three leading modes account for 79% of the variance. The first and third modes together explain 65% of the total variance. Their patterns (Figure 9a and 9c) present a cross-shore SLA gradient and

are therefore related to the along-shore circulation. Indeed, the sum of these modes is significantly correlated with the interannual satellite transport (0.76, 95% CL) and, not surprisingly, is significantly and negatively correlated to the SAM index (-0.5, 95% CL). The first mode explains 55.3% of the total variance and depicts a cross-shore SLA gradient. When this gradient is positive, the SLA is higher towards the coast and, consequently, the transport associated is towards the NE. This mode presents the strongest cross-shore gradients (0.65 cm / 100 km). The second mode (13.9% of the variance) shows along-shore SLA gradients that generate a cross-shore circulation. Although the SLA gradients of this mode are relatively weak (0.24 cm / 100 km), the associated circulation might have a key role in the exchange of water masses, nutrients, heat and salt between the coastal water and the outer shelf. Finally, the third mode explains 9.7% of the variance and represents cross-shore gradients of 0.40 cm / 100 km. The spatial pattern corresponding to the third mode presents a region with negative cross-shore gradient anomaly between the coast and A1 and a positive gradient between A1 and the shelf break. This result suggests a circulation anomaly cell with opposite velocity anomalies between the coast and A1 and between A1 and the shelf break.

The first EOF mode of the interannual SLA depicts very low SLA gradients and hence has a low impact in the local circulation. However, it explains, by far, the largest percentage of variance of the interannual SLA variability. We thus explore the physical processes responsible for the observed spatial pattern. At interannual and decadal timescales, it is known that SLAs are mainly modulated by the steric effect and the mass changes (Nerem et al., 2006). The steric effect accounts for changes in the salinity and temperature that impact on the SLA, while ocean mass changes induce changes in the Earth's gravity field which is accurately measured since 2003 by the Gravity Recovery and Climate Experiment (GRACE) satellite mission. Previous studies show that, in this region, the steric effect dominates the seasonal SLA changes (Ruiz-Etcheverry et al., 2016), but has no implications in the interannual component of the SLA (Combes & Matano, 2019). The first mode of the interannual SLA is correlated (0.5, 95% CL) with the first mode of the ocean mass changes measured by GRACE during the period 2003-2016 (Figure S7). Therefore, we conclude that the mass changes have a strong impact on the variability of the interannual SLA. A different and possible complementary explanation of this mode was provided by Combes & Matano (2019): they obtained a similar pattern for the first EOF mode of the interannual SLA over a wider region of the Patagonian shelf and attributed it to

the remote influence of the wind stress from offshore southern Chile. They also argued that the propagation of SSH anomalies from the Equatorial Pacific Ocean might modulate the SSH at these timescales. Despite of the possible origins of the first interannual SLA mode, we recall that it has no impact on the regional shelf circulation.

3.5 Relationship between the MC and the along-shelf transport variability

Previous studies based on numerical simulations suggest that the northeastward flow over the ACS between 38°S and 41°S is partly driven by the barotropic pressure gradients associated with variations in the strength of the MC (Palma et al., 2008; Matano et al., 2010). In this section we explore the possible relationship between the MC transport (Artana et al., 2018) and the satellite derived along-shore continental shelf transport described above (Figure 10). The correlation coefficients resulting from this comparison are significant at the 95% CL only within 30 km from the shelf break, suggesting that the MC impact is limited to a relatively narrow strip close the shelf break (Figure 10). The analysis of the coherence between the MC transport and the shelf transport (Figure S8) shows similar results: the MC and the along-shore transport are coherent only in the outer 30 km of the continental shelf for periods higher than 4 months. Palma et al. (2008) analyzed the continental shelf circulation based on numerical model outputs. They concluded that the MC variability affects the ACS circulation in the middle and outer shelf. However, in this study we observe that the influence of the MC variability over the along-shore circulation is restricted to the outer 30 km of the shelf. The difference observed might be due inaccuracies in the satellite data and/or in the different parameterizations that the model assumes (Palma et al., 2008). Further studies are necessary to explain the differences observed.

4 Conclusions

The present work reports the first estimate of the along-shore volume transport based on direct velocity observations in the northern portion of the Argentine continental shelf. The cross-shelf section considered to compute the transport is under track #26 of the Jason-2 satellite mission and extends between the coast and the 200 m isobath. Along this section, two bottom-mounted moorings and an oceanographic buoy were deployed between December 2014 and November 2015. To compute the transport these data were combined with sea level anomalies from satellite altimetry and a coastal tide gauge. The volume transport was computed using three different

methods: a direct method based on the direct velocity observations, an indirect method based on geostrophic velocities inferred from bottom pressure observations, and a satellite method based on geostrophic velocities derived from satellite altimetry data. The indirect and the satellite derived methods are only able to capture the geostrophic flow associated with cross-shore sea level gradients. However, the in situ (direct and indirect) transports present similar variability, suggesting that the barotropic component of the transport can be successfully determined from a few bottom pressure measurements, without the need of a denser horizontal sampling array. The cross-shore coherence of the along-shore flow in this portion of the shelf is also suggested, though less reliably, from satellite altimetry observations (7 km resolution, Strub et al., 2015) and high-resolution models (5 km resolution, Palma et al., 2008). Therefore, we argue that the number of instruments available is enough to obtain an accurate measure of the along-shore transport. The mean in situ transport is 2.65 Sv towards the northeast, which is larger than reported in previous studies, computed at other locations: 1.3 Sv (Forbes & Garraffo, 1988), 0.9 Sv (Palma et al., 2008) and 1.7 Sv (Combes & Matano, 2018). We are working in a complementary manuscript comparing in situ data with different model outputs. The in situ transport estimates present large variability, with a peak-to-peak range of 16 Sv, and several events of (southwestward) transport reversals lasting a few days. The transport resulting from the satellite method accurately reproduces the in situ transport variability. The best fit between satellite derived and in situ transports (mean difference 0.24 Sv) is obtained when using CENS2018 MDT.

The variability of the de-tided in situ transport is dominated by oscillations with periods between 2 and 5 days, a range typical of the atmospheric variability in this region. The along-shore wind stress induces a cross-shore Ekman transport which in turn sets up a cross-shore pressure gradient that modulates the geostrophic along-shore transport. This mechanism explains the high correlation ($r \sim 0.7$) between the along-shore in situ transport and the along-shore wind stress at the synoptic scale, but also between the 25-year satellite transport and the wind stress at interannual scales. The interannual component of the along-shore transport correlates significatively with the Southern Annular Mode, which dominates the interannual wind stress variability in the region. During the positive phase of the SAM, the along-shore southwesterly winds are weaker, leading to a decrease of the northeastward shelf transport. This suggests that the response of the shelf transport to wind variations resembles that of southern Patagonia

reported by recent studies. The 25-year satellite transport is dominated by the annual cycle, which ranges between 1 and 4 Sv and is maximum during the austral autumn and minimum in the austral spring. In situ monthly data shows that in July (September) 2015 the along-shore transport was substantially smaller (larger) than the climatological transport, in agreement with weaker (stronger) than usual southwesterly winds. We also show that the satellite along-shore transport is significantly correlated to the Malvinas Current transport only in a 30 km wide band along the shelf break. The leading mode of the interannual variability of SLA distribution is largely correlated to ocean mass changes. Yet, the associated spatial pattern does not present significant gradients and therefore does not impact on the circulation variability. Once the leading mode is filtered out from the interannual SLA, the remaining three leading modes exhibit SLA gradients associated with variations of the along-shore circulation (mode 1, 55.3%, and mode 3, 9.7% explained variance) and of the cross-shore circulation (mode 2, 13.9% explained variance). Despite the second and third mode explain a relatively small percentage of variance, the patterns displayed might have important consequences in both the circulation and ecosystem of the region.

Overall, we show that the geostrophic along-shore volume transport can be estimated with few in situ deployments and that the barotropic transport is dominated by the along-shore wind stress at the atmospheric synoptic and interannual time scales. We also show that it is possible to monitor the transport, at time-scales longer that 20-days, with satellite altimetry data.

Acknowledgments

This work was supported by European Organisation for the Exploitation of Meteorological Satellites (EUMETSAT)/Centre National de la Recherche Spatial (CNES) through project DSP/OT/07-2118 and by Agencia Nacional de Promoción Científica y Tecnológica (Argentina), project PICT 2018-02433. ARP acknowledges the support from the Inter-American Institute for Global Change Research grant CRN3070, which is supported by the US National Science Foundation grant GEO-1128040.

The tide gauge data from Mar del Plata were kindly provided by the Tide Section of the Oceanography Department, Servicio de Hidrografía Naval (Argentina). It is also publicly available at https://uhslc.soest.hawaii.edu/datainfo/. In situ data analyzed in this study within

CASSIS proyect can be found in public SEANOE public data repository at https://www.seanoe.org/data/00403/51492/ and https://www.seanoe.org/recordview. The gridded satellite altimetry product is available at http://marine.copernicus.eu/, and the along-track satellite product, at https://openadb.dgfi.tum.de/en/. The ERA-Interim reanalysis data can be found at https://www.ecmwf.int/.

References

Acha, E. M., Mianzan, H. W., Guerrero, R. A., Favero, M., & Bava, J. (2004). Marine fronts at the continental shelves of austral South America: Physical and ecological processes. *Journal of Marine systems*, *44*(1-2), 83-105. https://doi.org/10.1016/j.jmarsys.2003.09.005

Álvarez-Colombo, G., Dato, C., Macchi, G. J., Palma, E., Machinandiarena, L., Christiansen, H. E., ... & Brown, D. (2011). Distribution and behavior of Argentine hake larvae: Evidence of a biophysical mechanism for self-recruitment in northern Patagonian shelf waters. Ciencias Marinas, 37(4B), 633-657. https://www.redalyc.org/articulo.oa?id=48021256009

Andersen, O., Knudsen, P., & Stenseng, L. (2015). The DTU13 MSS (mean sea surface) and MDT (mean dynamic topography) from 20 years of satellite altimetry. In *IGFS* 2014 (pp. 111-121). Springer, Cham. https://doi.org/10.1007/1345_2015_182

Artana, C., Ferrari, R., Koenig, Z., Sennéchael, N., Saraceno, M., Piola, A. R., & Provost, C. (2018). Malvinas Current volume transport at 41 S: A 24 yearlong time series consistent with mooring data from 3 decades and satellite altimetry. *Journal of Geophysical Research: Oceans*, 123(1), 378-398. https://doi.org/10.1002/2017JC013600

Auad, G., & Martos, P. (2012). Climate variability of the northern Argentinean shelf circulation: Impact on Engraulis Anchoita. *The International Journal of Ocean and Climate Systems*, *3*(1), 17-43. https://doi.org/10.1260/1759-3131.3.1.17

Bakun, A. (1996). Patterns in the ocean: ocean processes and marine population dynamics. California Sea Grant, in cooperation with Centro de Investigaciones Biologicas del Noroeste, La Paz, Mexico.

Ballarotta, M., Ubelmann, C., Pujol, M. I., Taburet, G., Fournier, F., Legeais, J. F., ... & Picot, N. (2019). On the resolutions of ocean altimetry maps. *Ocean Science*, 15(4), 1091-1109. https://doi.org/10.5194/os-2018-156

Berden, G., Charo M., Möller Jr., O. O., Piola A. R. (2020). Circulation and Hydrography in the western South Atlantic shelf and export to the deep adjacent ocean -30 to 40°S. Journal of Geophysical Research: Oceans.

Berrisford, P., Dee, D. P. K. F., Fielding, K., Fuentes, M., Kallberg, P., Kobayashi, S., et al. (2009). The ERA-interim archive. *ERA report series*, (1), 1-16, ECMWF: Reading, UK. Retrieved from www.ecmwf.int/publications

Birol, F., Fuller, N., Lyard, F., Cancet, M., Nino, F., Delebecque, C., ... & Léger, F. (2017). Coastal applications from nadir altimetry: example of the X-TRACK regional products. *Advances in Space Research*, 59.4: 936-953. https://doi.org/10.1016/j.asr.2016.11.005

Brink, K.H. (2016). Cross-shelf exchange. *Annual review of marine science*, 8, pp.59-78.

Brun, A.A., Ramirez, N., Pizarro, O. and Piola, A.R., 2020. The role of the Magellan Strait on the southwest South Atlantic shelf. Estuarine, *Coastal and Shelf Science*, p.106661. https://doi.org/10.1016/j.ecss.2020.106661

Combes, V., & Matano, R. P. (2018). The Patagonian shelf circulation: Drivers and variability. *Progress in oceanography*, *167*, 24-43. https://doi.org/10.1016/j.pocean.2018.07.003

Combes, V., & Matano, R. P. (2019). On the origins of the low-frequency sea surface height variability of the Patagonia shelf region. *Ocean Modelling*, 142, 101454. https://doi.org/10.1016/j.ocemod.2019.101454

Ferrari, R., Artana, C., Saraceno, M., Piola, A. R., & Provost, C. (2017). Satellite altimetry and current-meter velocities in the Malvinas Current at 41° S: Comparisons and modes of variations. *Journal of Geophysical Research: Oceans*, 122(12), 9572-9590. https://doi.org/10.1002/2017JC013340

Forbes, M. C., & Garraffo, Z. D. (1988). A note on the mean seasonal transport on the Argentinian Shelf. *Journal of Geophysical Research: Oceans*, 93(C3), 2311–2319. https://doi.org/10.1029/JC093iC03p02311

GEBCO, C. (2003). General Bathymetric Chart of the Ocean. *British Oceanographic Data Center*. Monaco, International Hydrographic Organization.

Guerrero, R. A., & Piola, A. R. (1997). Masas de agua en la plataforma continental.

Guihou, K., Piola, A.R., Palma, E.D. & Chidichimo, M.P. (2019). Dynamical Connections between Large Marine Ecosystems of Austral South America based on numerical simulations, *Ocean Science*. https://doi.org/10.5194/os-16-271-2020

Lago, L. S., Saraceno, M., Martos, P., Guerrero, R. A., Piola, A. R., Paniagua, G. F., ... & Provost, C. (2019). On the wind contribution to the variability of ocean currents over wide continental shelves: a case study on the northern Argentine continental shelf. *Journal of Geophysical Research: Oceans*. https://doi.org/10.1029/2019JC015105

Lago, L. S., Saraceno, M., Ruiz-Etcheverry, L. A., Passaro, M., Oreiro, F. A., D'Onofrio, E. E., & González, R. A. (2017). Improved sea surface height from satellite altimetry in coastal zones: A case study in Southern Patagonia. *IEEE Journal of Selected Topics in Applied Earth Observations and Remote Sensing*, 10(8), 3493-3503. https://doi.org/10.1109/JSTARS.2017.2694325

Marshall, G. J. (2003). Trends in the Southern Annular Mode from observations and reanalyses. *Journal of Climate*, 16(24), 4134-4143. https://doi.org/10.1175/1520-0442(2003)016<4134:TITSAM>2.0.CO;2

Matano, R., Palma, E. D., & Piola, A. R. (2010). The influence of the Brazil and Malvinas Currents on the Southwestern Atlantic Shelf circulation. *Copernicus Publications, Ocean Science (os), 6*, 983-995. http://dx.doi.org/10.5194/os-6-983-2010

Maximenko, N., P. Niiler, L. Centurioni, M. Rio, O. Melnichenko, D. Chambers, V. Zlotnicki, and B. Galperin, 2009: Mean Dynamic Topography of the Ocean Derived from Satellite and Drifting Buoy Data Using Three Different Techniques. J. Atmos. *Oceanic Technol.*, 26, 1910–1919, https://doi.org/10.1175/2009JTECHO672.1

Meinen, C. S., & Watts, D. R. (2000). Vertical structure and transport on a transect across the North Atlantic Current near 42 N: Time series and mean. *Journal of Geophysical Research: Oceans*, 105(C9), 21869-21891. https://doi.org/10.1029/2000JC900097

Meinen, C. S., Baringer, M. O., & Garcia, R. F. (2010). Florida Current transport variability: An analysis of annual and longer-period signals. *Deep Sea Research Part I: Oceanographic Research Papers*, 57(7), 835-846. https://doi.org/10.1016/j.dsr.2010.04.001

Nerem, R. S., Leuliette, E., & Cazenave, A. (2006). Present-day sea-level change: A review. *Comptes Rendus Geoscience*, 338(14-15), 1077-1083. https://doi.org/10.1016/j.crte.2006.09.001

Palma, E. D., Matano, R. P., & Piola, A. R. (2008). A numerical study of the Southwestern Atlantic Shelf circulation: Stratified ocean response to local and offshore forcing. *Journal of Geophysical Research: Oceans*, *113*(C11). https://doi.org/10.1029/2007JC004720

Paniagua, G. F., Saraceno, M., Piola, A. R., Guerrero, R., Provost, C., Ferrari, R.,et al. (2018). Malvinas Current at 40° S–41° S: First Assessment of Temperature and Salinity Temporal Variability. *Journal of Geophysical Research: Oceans*, *123*(8), 5323-5340. https://doi.org/10.1029/2017JC013666

Passaro, M., Cipollini, P., Vignudelli, S., Quartly, G. D., & Snaith, H. M. (2014). ALES: A multi-mission adaptive subwaveform retracker for coastal and open ocean altimetry. *Remote Sensing of Environment*, 145, 173-189.

Piola, A. R., & Rivas, A. (1997). Corrientes en la plataforma continental.

Piola, A. R., Campos, E. J., Möller, O. O., Charo, M., & Martinez, C. (2000). Subtropical shelf front off eastern South America. *Journal of Geophysical Research: Oceans*, *105*(C3), 6565-6578. https://doi.org/10.1029/1999JC000300

Piola, A. R., R. P. Matano, E. D. Palma, O. O. Moller Jr., and E. J. D. Campos (2005), The influence of the Plata River discharge on the western South Atlantic shelf, *Geophys. Res. Lett.*, 32, L01603, https://doi.org/10.1029/2004GL021638

Piola, A. R., Romero, S. I., & Zajaczkovski, U. (2008). Space–time variability of the Plata plume inferred from ocean color. *Continental Shelf Research*, *28*(13), 1556-1567. https://doi.org/10.1016/j.csr.2007.02.013

Preisendorfer, R.W., 1988. Principal component analysis in meteorology and oceanography. (Ed.: Mobley, C.D.), *Developments in Atmospheric Science*, 17, Elsevier, Amsterdam, 425 pp.

Rio M. H., Guinehut S., & Larnicol G. (2011). The New CNES-CLS09 global Mean Dynamic Topography computed from the combination of GRACE data, altimetry and in-situ measurements. J. Geophys. Res., 116, C07018, https://doi.org/10.1029/2010JC006505

Rivas, A.L. (1994). Spatial variation of the annual cycle of temperature in the Patagonian shelf between 40 and 50 of south latitude. *Continental Shelf Research*, 14(13-14), pp.1539-1554. https://doi.org/10.1016/0278-4343(94)90089-2

Romero, S. I., Piola, A. R., Charo, M., & Garcia, C. A. E. (2006). Chlorophyll-a variability off Patagonia based on SeaWiFS data. *Journal of Geophysical Research: Oceans*, 111(C5). https://doi.org/10.1029/2005JC003244

Ruiz-Etcheverry, L. A., Saraceno, M., Piola, A. R., & Strub, P. T. (2016). Sea level anomaly on the Patagonian continental shelf: Trends, annual patterns and geostrophic flows. *Journal of Geophysical Research: Oceans, 121*(4), 2733-2754. https://doi.org/10.1002/2015JC011265

Saraceno, M., Guerrero, R., Piola, A. R., Provost, C., Perault, F., Ferrari, R., et al. (2017). Malvinas Current 2014–2015: Mooring velocities. SEANOE. https://doi.org/10.17882/51492

Saraceno M., Guerrero, R., Piola, A. R., Provost, C., Perault, F., Ferrari, R., et al. (2019). Argentine continental shelf currents 2014-2015: velocities, pressure and temperature. SEANOE. https://doi.org/10.17882/61777

Saraceno, M., Simionato, C. G., & Ruiz-Etcheverry, L. A. (2014). Sea surface height trend and variability at seasonal and interannual time scales in the Southeastern South American continental shelf between 27 S and 40 S. *Continental Shelf Research*, 91, 82-94. https://doi.org/10.1016/j.csr.2014.09.002

Simpson, J.H. & Sharples, J. (2012). Introduction to the physical and biological oceanography of shelf seas. Cambridge University Press.

Strub, P. T., Chereskin, T. K., Niiler, P. P., James, C., & Levine, M. D. (1997). Altimeter-derived variability of surface velocities in the California Current System: 1. Evaluation of TOPEX altimeter velocity resolution. *Journal of Geophysical Research: Oceans*, 102(C6), 12727-12748. https://doi.org/10.1029/97JC00448

Strub, P. T., James, C., Combes, V., Matano, R. P., Piola, A. R., Palma, E. D., et al. (2015). Altimeter-derived seasonal circulation on the southwest Atlantic shelf: 27°–43° S. *Journal of Geophysical Research: Oceans*, *120*(5), 3391-3418. https://doi.org/10.1002/2015JC010769

Vignudelli, S., Kostianoy, A. G., Cipollini, P., & Benveniste, J. (Eds.). (2011). Coastal altimetry. Springer, Berlin, Heidelberg.

Figure 1. Location of the moorings (black dots): A1 and A2 are bottom-mounted upward-looking ADCPs, TG is the tide gauge located in Mar del Plata and oceanographic buoy. See Section 2 for further details. White lines are isobaths from the General Bathymetric Chart of the Ocean (GEBCO, 2003) combined with the bathymetry measurements from Servicio de Hidrografia Naval (SHN, Argentina), with the thick line indicating the 200 m isobath. The red line indicates Jason-2 track #26 and the black arrows are schematic representations of the Malvinas (MC) and Brazil (BC) Currents. The background colors show the Reynolds SST climatology between 1993 and 2017 (https://podaac-tools.jpl.nasa.gov).

Table 1. In situ period of measurement (days), depth at the location of the moorings (m) and mean and std of the along-shore and cross-shore velocity (cm s^{-1}) for each instrument.

Figure 2. Schematic cross-shelf section along the mooring line. Areas used for the direct (a) and indirect (b) transport estimate methods based on in situ observations. A1 and A2 indicate the location of the upward-looking ADCPs; The location of the oceanographic buoy, TG and A1 and A2 moorings are indicated by red dots. X1 and X2 indicate the mid-points between the pressure measurements used to estimate the geostrophic velocities between TG and A1 and between A1 and A2, respectively.

Figure 3. Along-shore direct (blue) and indirect (red) transport estimates (in Sv) using in situ observations. The transport is calculated across the section of the continental shelf between the coast and the 200 m isobath under Jason 2 track #26. See text for explanation on the methodology (Section 2). The gray shading represents the standard deviation.

Figure 4. Along-shore direct transport (black) and along-shore wind stress (magenta), representative of Area1_1 (a), Area2_1 (b) and Area3_1 (c) as indicated in Figure 2a.

Table 2. Correlation coefficient and RMSE (cm s^{-1}) between the in situ along-shore velocities at specified locations (X1, A1, X2, A2) and the along-shore velocities from the AVISO L4 multi-satellite gridded product. In situ time series were low-pass filtered with different a cut-off period of 20 days. All correlation coefficients are significant at a 95% CL.

Figure 5. (a) Along-shore direct transport estimate for the period of in situ observations (magenta) and satellite transport from velocities inferred from AVISO L4 gridded SSH

computed using CNES2018 MDT (black). A low-pass filter with a cut-off period of 20 days was applied to the in situ time series. (b) Along-shore transport time series derived from satellite altimetry data for the period 1993-2017 (black). Overlapped is the transport from in situ measurements during the period December 2014 to November 2015 (magenta).

Figure 6. Power density spectrum [Sv^2 day] in logarithmic scale of the along-shore satellite transport based on the 25-year satellite altimetry record. The dashed line is the null continuum and the dot lines are the 95% confidence levels.

Figure 7: (a) Monthly climatology (black) and standard deviation (grey shading) of the along-shore satellite transport for the period 1993-2017. The monthly mean of the satellite along-shore transport in 2015 is shown in magenta. (b) Monthly climatology (black) and standard deviation (grey shading) of the ERA-Interim along-shore wind stress for the period 1993-2017. The monthly mean of the ERA-Interim wind stress for 2015 is shown in magenta.

Figure 8. Interannual component of the along-shore satellite transport (black) and the interannual component of the SAM index (magenta). Note that the SAM index scale (right axes) is reversed. The correlation coefficient between the SAM index and the along-shore satellite transport is -0.5.

Figure 9: First (a), second (b) and third (c) EOF modes [cm] of the interannual SLA residual and (d, e, f) their corresponding time series. The percentage of variance explained by each mode is indicated above panels a-c.

Figure 10. Correlation coefficient between the satellite derived along-shore component of the MC transport and the along-shore transport along the ACS based on the 1993-2017 altimetry data. Dashed lines indicate the 95% confidence level.

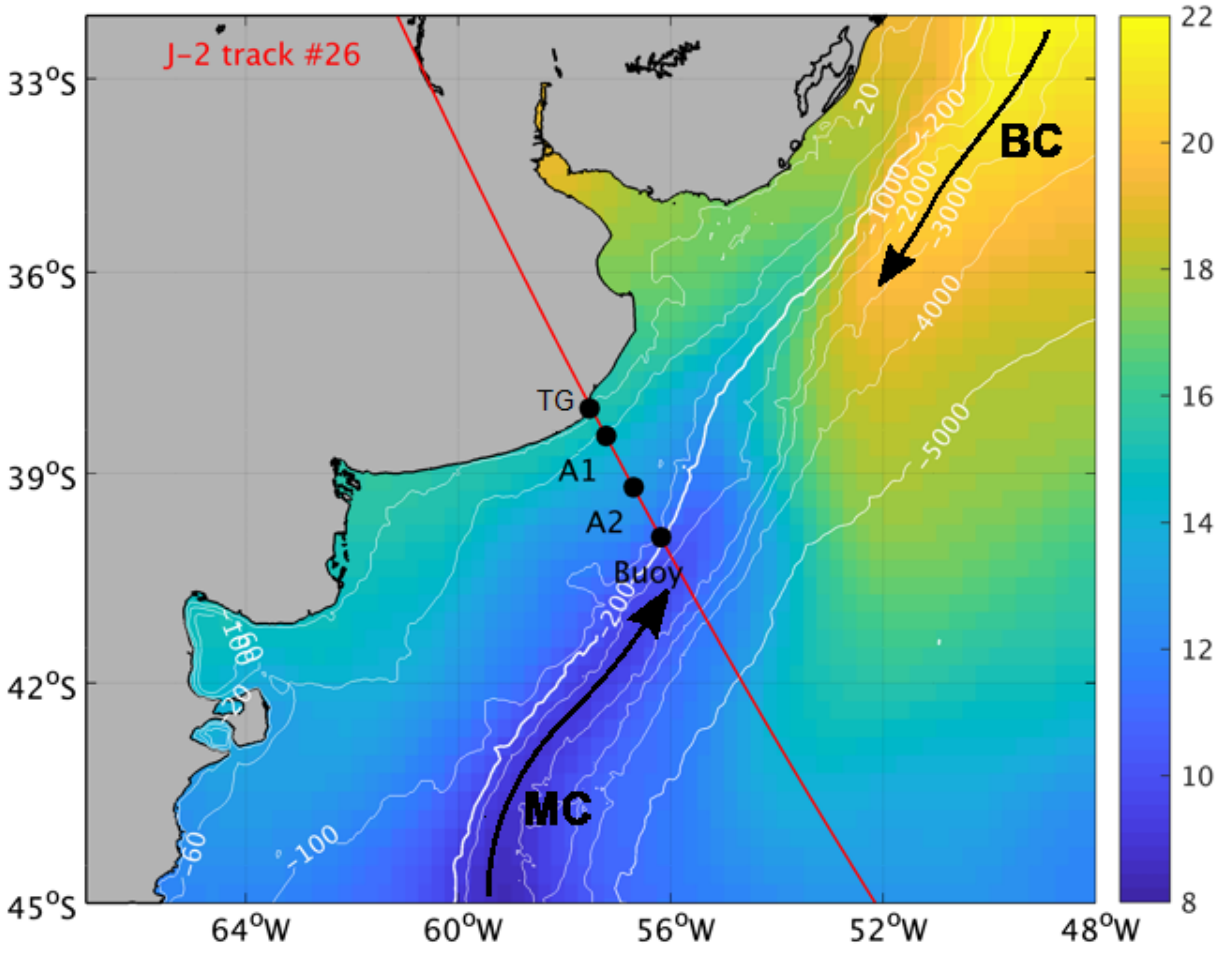

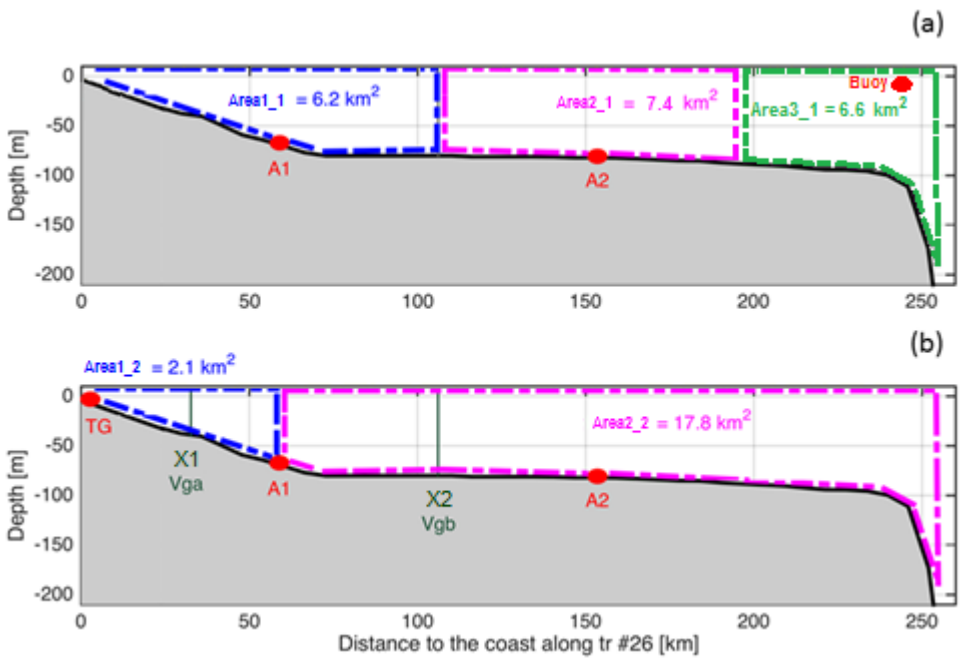

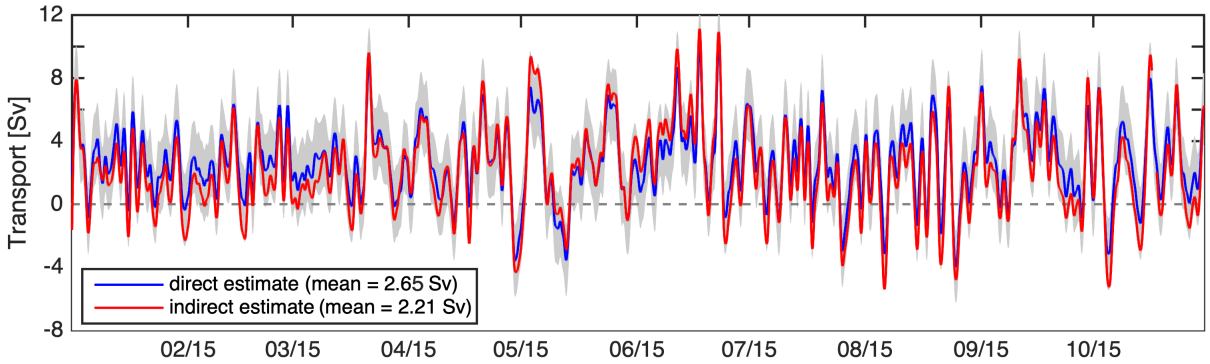

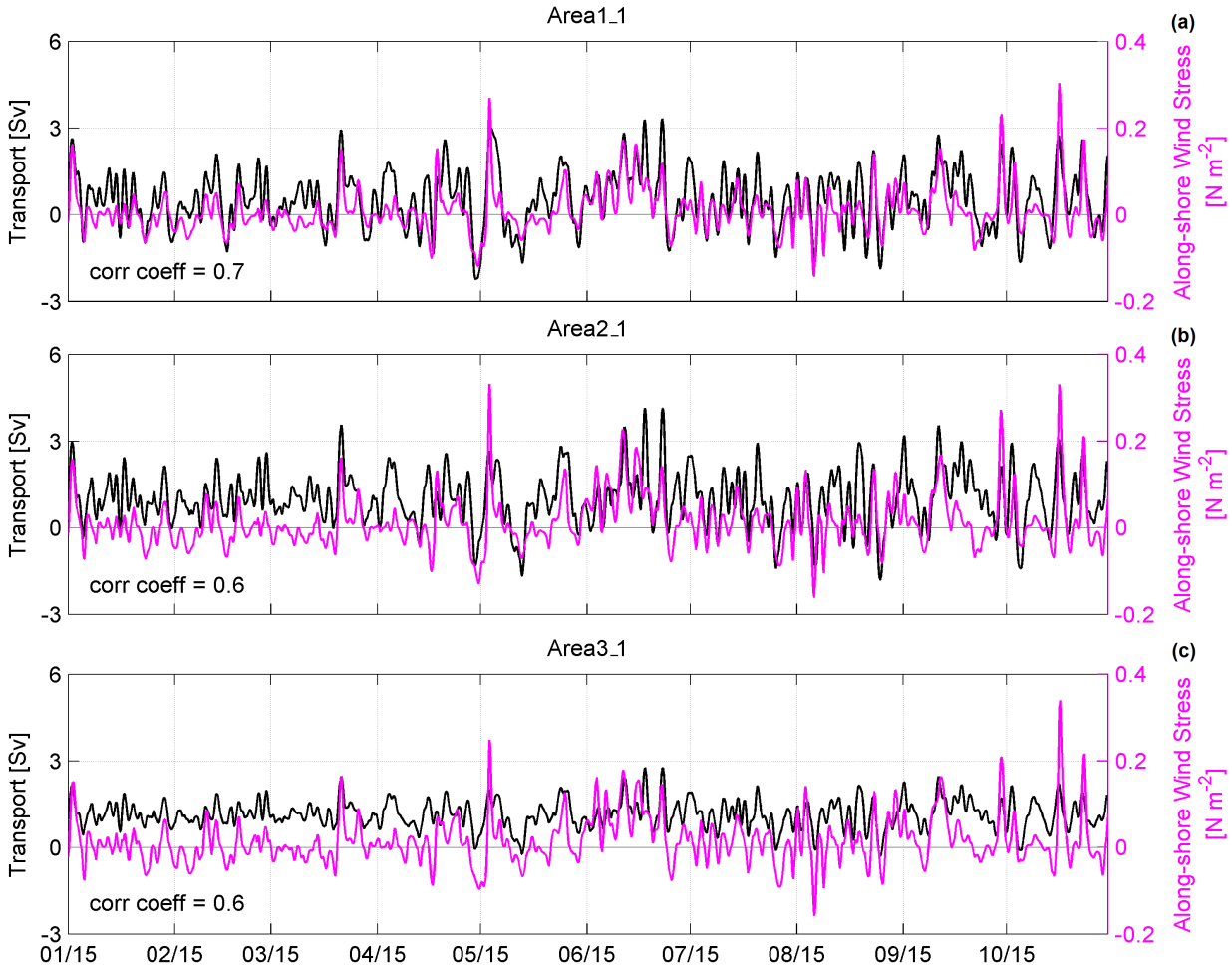

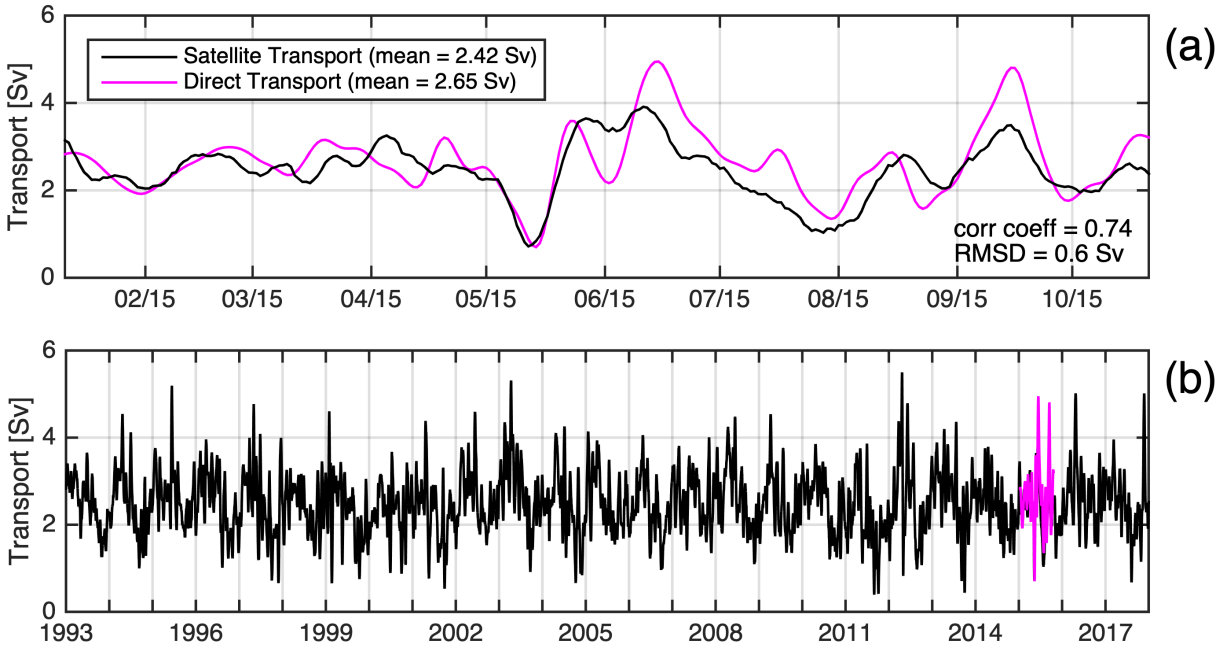

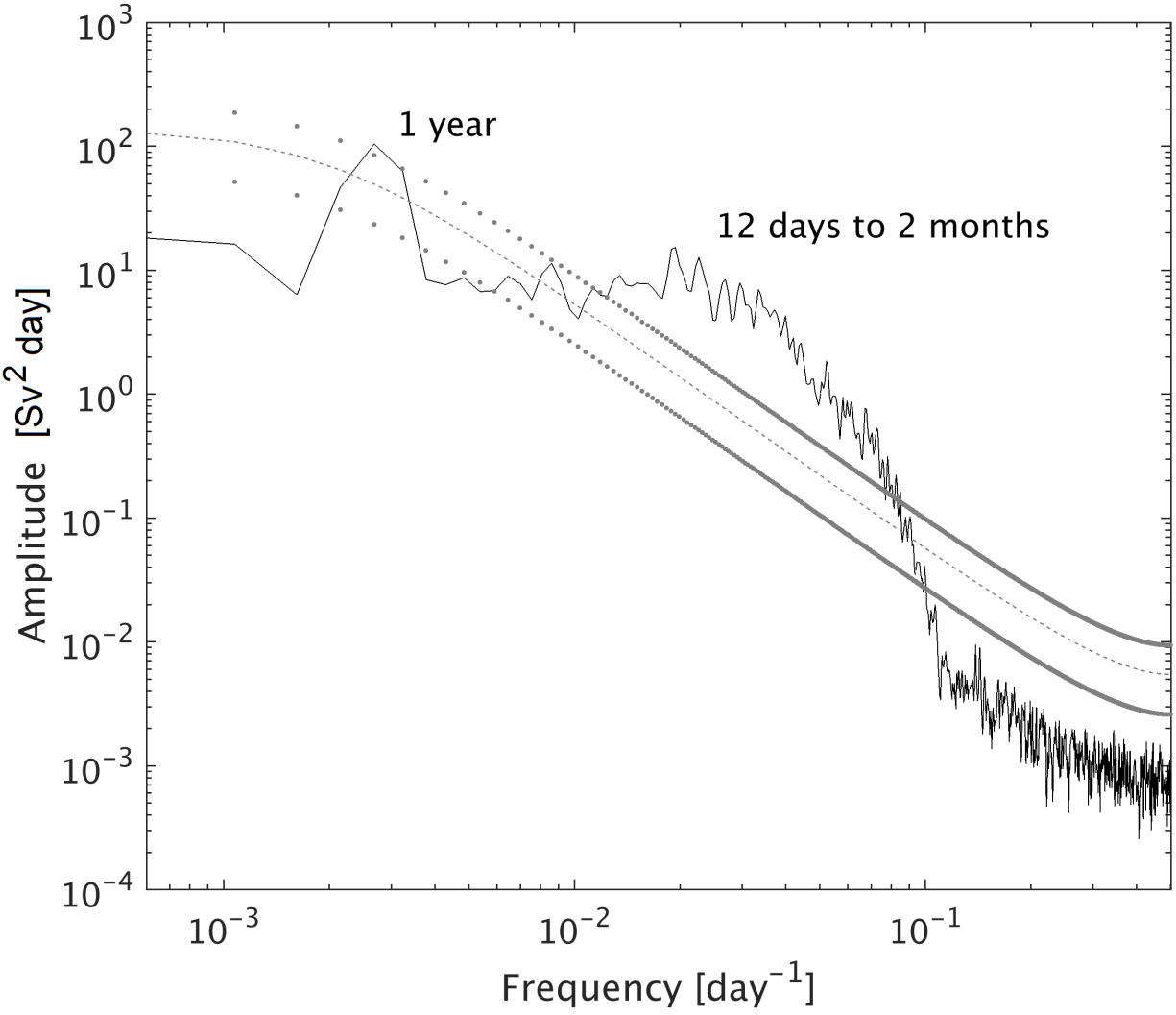

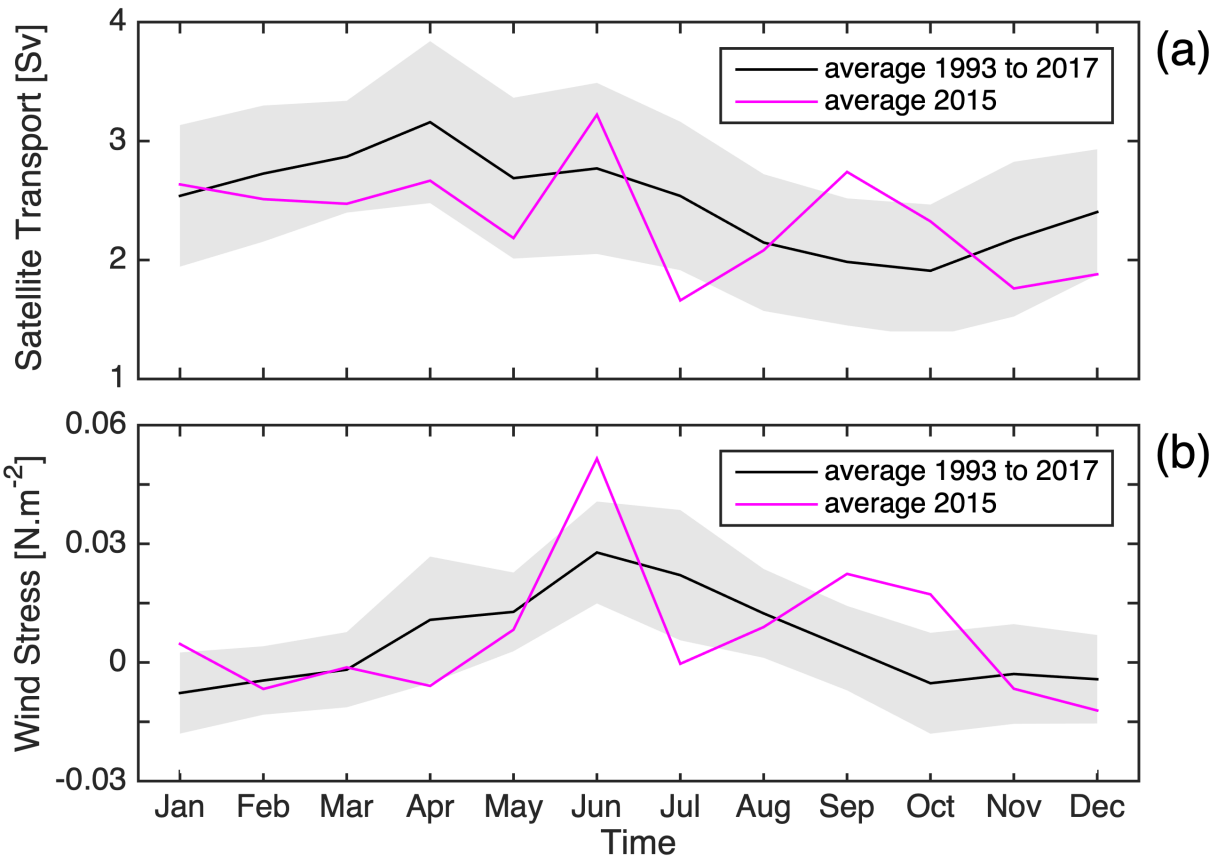

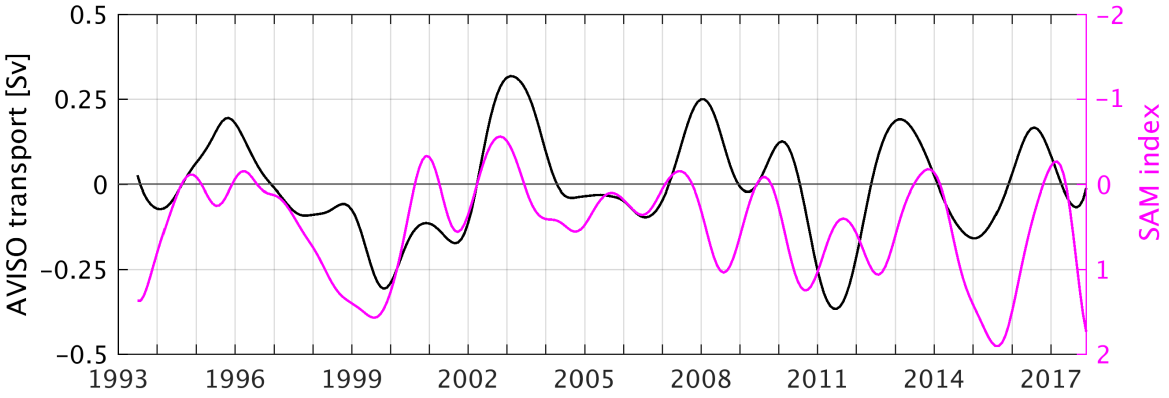

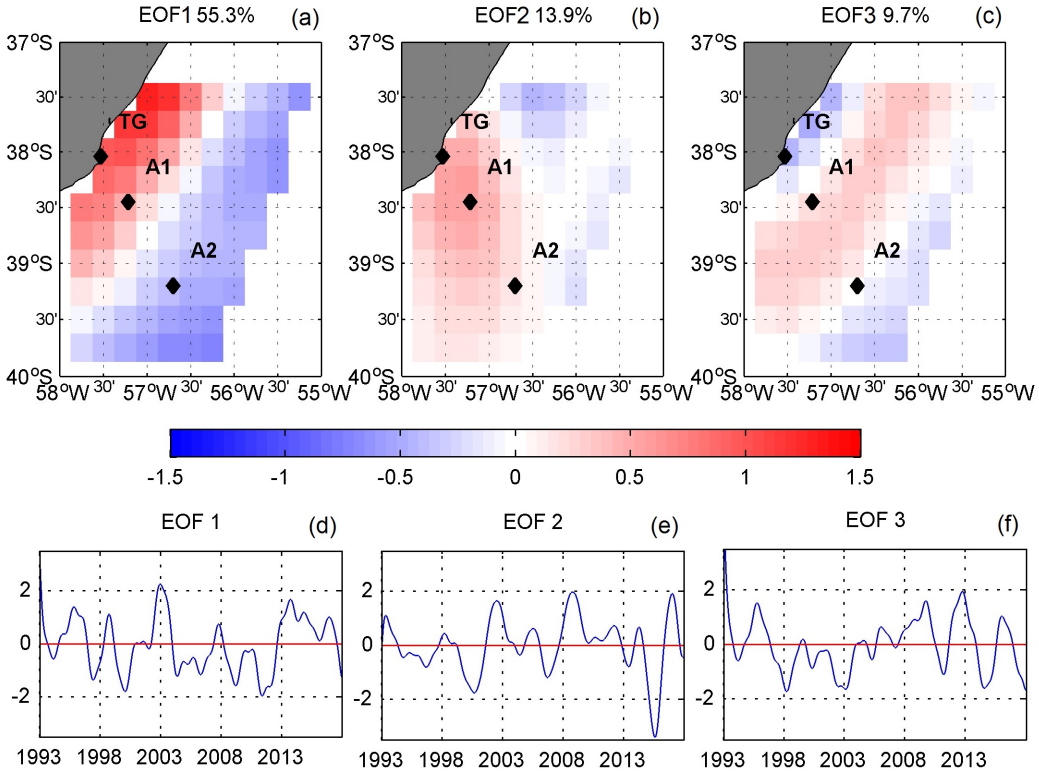

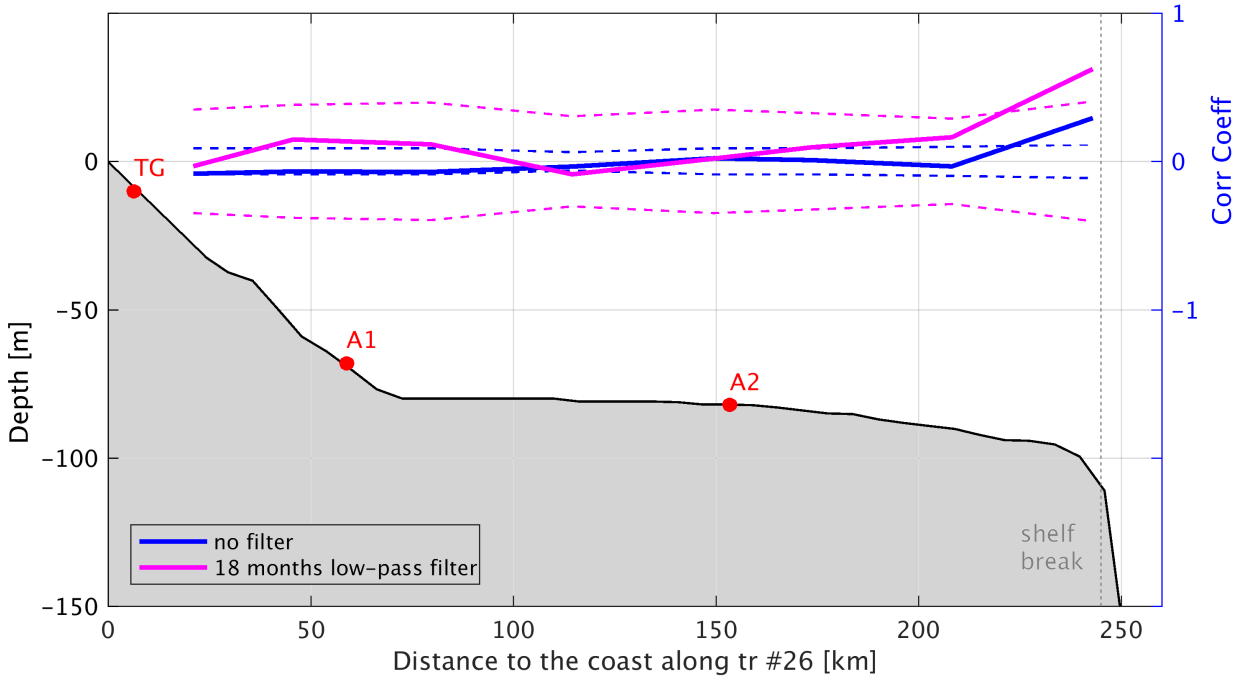

	Start	End	Depth (m)	Duration (days)	Along-shore vel (cm s^{-1})		Cross-shore vel (cm s^{-1})	
					mean	std	mean	std
TG	12/17/2014	11/21/2015	0	340	-	-	-	-
A1	12/17/2014	11/18/2015	70	337	8.4	15.8	-0.4	3.6
A2	12/17/2014	11/17/2015	90	336	13.3	12.3	2.9	3.5
Buoy	12/21/2014	01/31/2015	200	42	16.5	4.8	6.2	3.8

	Corr Coeff	RMSE (cm s^{-1})
X1	0.4	9
A1	0.7	5
X2	0.8	4
A2	0.7	3